Airgap-harmonic-oriented Partitioned Design Method of PMV Motor with Improved Torque Performances

Zhaopeng Wu, Li Quan, Zixuan Xiang, *Member, IEEE,* Deyang Fan, Tengguang Wang, and Xiaoyong Zhu

***Abstract*—Here, we introduce a partitioned design method that is oriented toward airgap harmonic for permanent magnet vernier (PMV) motors. The method proposes the utilization of airgap flux harmonics as an effective bridge between the torque design region and the torque performances. To illustrate the efficacy of this method, a partitioned design PMV motor is presented and compared with the initial design. Firstly, the torque design region of the rotor is artfully divided into the torque enhancement region and ripple reduction region. Meanwhile, the main harmonics that generate output torque are chosen and enhanced, optimization. Moreover, the harmonics that generate torque ripple are selected and reduced based on torque harmonics optimization. Finally, the functions of the partitioned PMV motor torque are assessed based on the finite element method. By the purposeful design of these two regions, the output torque is strengthened while torque ripple is inhibited effectively, verifying the effectiveness and reasonability of the proposed design method.**

***Index Terms*—Permanent magnet vernier (PMV) motor, Airgap flux harmonic, Partitioned design, Low torque ripple.**

I. Introduction

PERMANENT magnet vernier (PMV) motor has become an excellent candidate in various industries due to its inherent abilities, such as exhibiting low-velocity high-torque. Fig. 1 shows some industries, such as electric vehicles, wind energy, and boat power [1]-[3]. The double-stator permanent magnet vernier motor has been recommended to meet the rising market need for torque output capacity machines [4] as this has been shown to effectively reduce flux leaks and remarkedly improve PM use due to its high-torque abilities. It is noted that, due to the unique double stator structure, there are two layers of airgap in the motor, which inevitably leads to a complex structure and increased assembly difficulty. Based on this, the winding construction with auxiliary DC-field excitation is adopted to achieve good torque performance in [5]. However, this leads to a significant increase in control problems. Thus, enhancing the performances of PMV motors, despite being a pressing and difficult issue to tackle, remains a research hotspot.

Generally, with the increasing critical demand for electric vehicle drives, there are a variety of design requirements for performance, especially output torque and torque ripple [6]. Many researchers are striving to discover new torque performance enhancement techniques. In this regard, the high torque density flux modulated permanent magnet (FMPM) motor with non-uniform modulated teeth was developed in [7]. Its torque is significantly higher than that of traditional motors. At the same time, the winding design of a double salient pole permanent magnet motor with a magnetic modulation effect is studied, and the winding span and slot angle are cleverly designed [8]. Thus, its generated torque is remarkedly improved due to the winding design. Besides, a 26-pole PMVM possessing coding-sharped teeth has also been recommended [9] for its capability to induce permeance harmonics with specific phases and amplitude to obtain higher output torque. However, when using the above design method, it is inevitable to increase the torque ripple while increasing the output torque. In addition, other minimizing approaches, for instance, the skewed PM and eccentric PM in the PM rotor, have also been described [10]-[12] and were shown effective in reducing torque ripples due to modified PM topology and lower PM cogged torque. [13] Despite its complexity, a multi-harmonic injection method considering the harmonic phase angle for a surface-inset permanent magnet (SIPM) motor that can efficiently reduce torque ripples has also been investigated and shown promising results. Meanwhile, fabrication difficulties are increased due to the complex design. Consequently, it remains a hot focus for the study of torque performances of PMV motors and is full of challenges.

Here, we introduce an airgap-harmonic-orientated partitioned design method for increasing output torque and reducing torque ripples. In addition, on the basis of different harmonic effects on torque output, the torque design region of the rotor is artfully divided into the torque enhancement region and ripple reduction region. Moreover, the purposeful design of these two regions increases torque while reducing the corresponding ripples effectively. The paper is organized as follows. Section II describes and compares the differences between the initial motor with our proposed one on the basis

Manuscript received February 24, 2023; revised April 3, 2023; accepted April 25, 2023. Date of publication March 25. 2024; Date of current version February 20, 2024.

This work was supported in part by the Natural Science Foundation of China under Grant 51991385, Grant 52177046. (*Corresponding Author*: *Li Quan*)

Zhaopeng Wu, Li Quan, Zixuan Xiang, Deyang Fan, Tengguang Wang and Xiaoyong Zhu are with the School of Electrical and Information Engineering, Jiangsu University, Zhenjiang 212013, China (e-mail: 2222007122@stmail.ujs.edu.cn; quanli@ujs.edu.cn; zxxiang@ujs.edu.cn; fandeyang1004@163.com; 2112007007@stmail.ujs.edu.cn; zzyff@ujs.edu.cn;

Digital Object Identifier 10.30941/CESTEMS.2024.00002

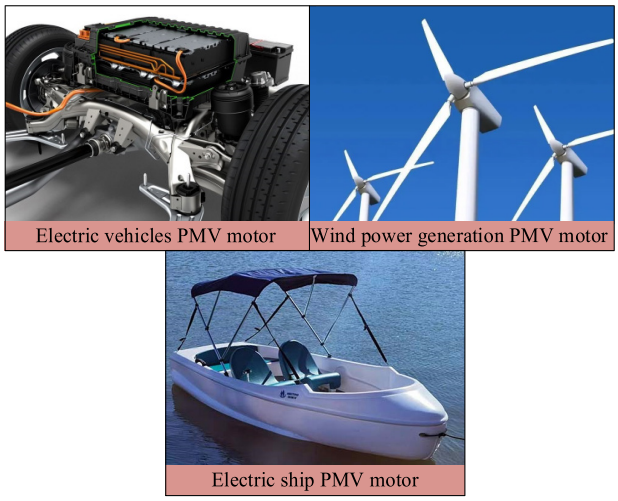

Fig. 1. The application of PMV motors in different industries.

of operating principles and describes the airgap-harmonic-orientated partitioned design principle. Section III illustrates techniques implemented to optimize our proposed airgap-harmonic-orientated partitioned design method. Lastly, Section IV accounts for the three motors' electromagnetic performances using finite element analysis (FEA), and Section V concludes the entire airgap-harmonic-orientated partitioned design method.

II. Motor Configuration and Torque Improvement Method

A. Motor Configurations

The V-shaped permanent magnet vernier (PMV) motor is investigated, and its framework is shown in Fig. 2(a). It comprises a 19-pole pair outer PM rotor (V-shaped topology) and a 12-slot inner stator. Its three-phase armature winding with pole pair no. 5 is wound on the slotted stator core. Notably, a prototype PMV motor has also been designed (Fig. 2(b)), and its basic parameters are illustrated in Table I. Fig. 2(c) depicts the corresponding experiment platform, including the V-shaped PMV motor, torque sensor, magnetic powder brake, and optical-electricity encoder.

Fig. 3 shows the steady torque performances of this PMV motor are tested. It can be seen from the test results that the manufactured motor exhibits desirable output torque, but the corresponding torque ripple is up to 8.7%, which deserves further improvement.

TABLE I
MAIN DESIGN PARAMETERS OF THE INITIAL PMV MOTOR

Parameters	Value
Rated current (A)	25
Rated voltage (V)	90
Rated speed (r/min)	316
Slot/pole-pair number	12/19
Pole pair number of winding	5
Turns per phase	114
Airgap length (mm)	0.6
Outer radius of rotor (mm)	110
Outer radius of stator (mm)	90.25
Stack length (mm)	60

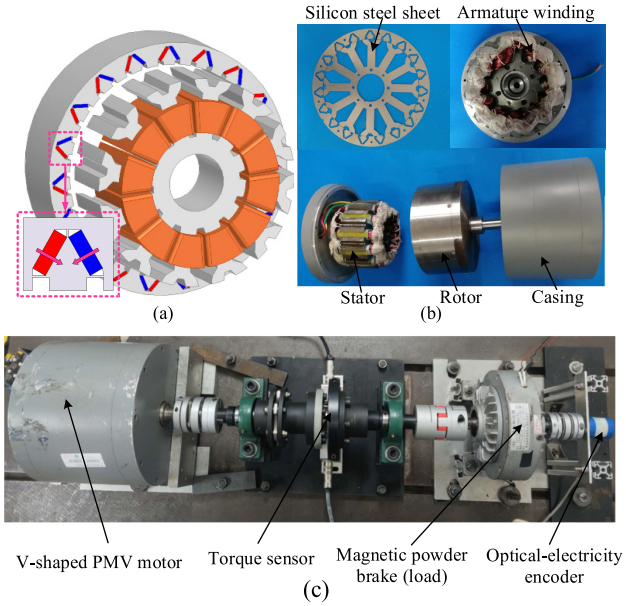

Fig. 2. (a) Motor configuration. (b) Components of the prototype motor. (c) Experiment platform.

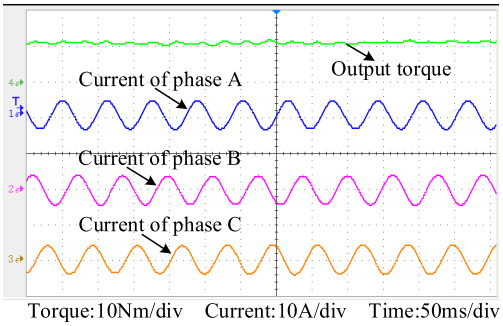

Fig. 3. Measured steady-state torque.

B. Airgap-harmonic-oriented Partitioned Design Method

Fig. 4 shows our proposed method for the PMV motor, which has some advantages compared to traditional design methods. Firstly, its airgap flux harmonics were creatively considered during the designing stage and bridged the torque design region with the motor performance. Secondly, considering the influence of different harmonics on torque performances, the torque design region of the rotor is skillfully divided into the torque enhancement region and the ripple reduction region. We obtained increased torque output and reduced torque ripples through the targeted design of these two regions. Finally, by using the suitable optimization algorithm, the airgap flux harmonics can be enhanced effectively if they positively impact motor performances, and will be suppressed if they negatively affect motor performances. Hence, our proposed airgap-harmonic-oriented partitioned methodology establishes a relationship among the design region, airgap flux harmonics, and torque output, which can be helpful to the high-quality design of PMV motors.

To compare and highlight the promising effects of the partitioned design method, this paper presents Motor 1(without partitioned design) and Motor 3(with partition design) for comparison with the investigated prototype (Motor

2). Fig. 5(a) shows Motor 1, and Fig. 5(b) shows the proposed partitioned design PMV motor. At the same time, the division of the torque design region of the PMV motor in the partitioned design is shown in Fig. 5(c).

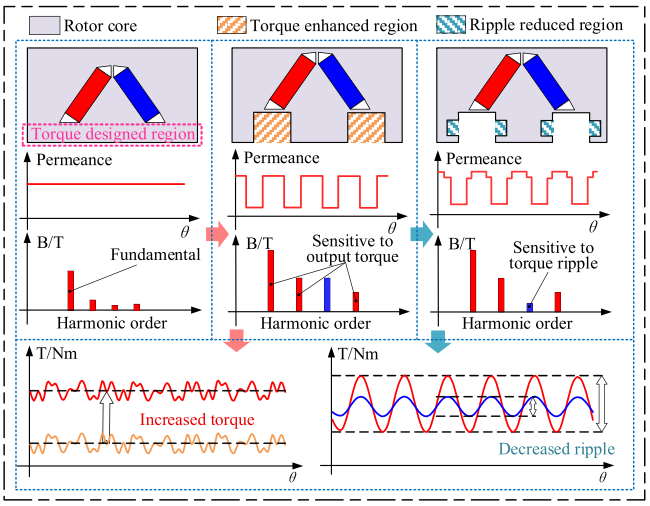

Fig. 4. Principle of partition design of PMV motors.

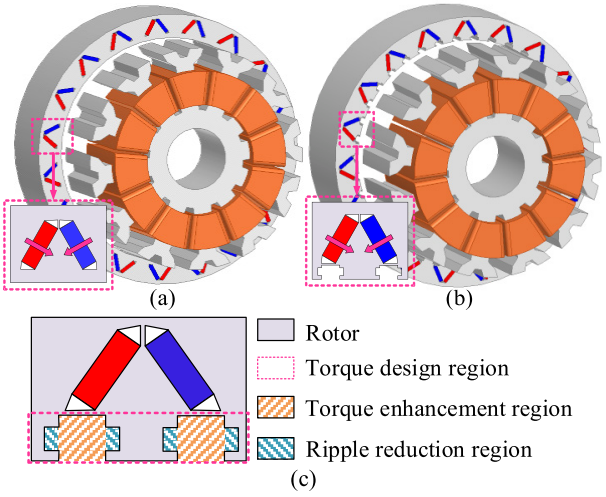

Fig. 5. (a) Configuration of Motor 1. (b) Configuration of Motor 3. (c) The division of torque design region.

C. Working Principle

The proposed partitioned design PMV motor can obtain larger torque density than traditional PM one due to magnetic field modulation effects. The magnetic field modulation effects of the proposed partitioned design PMV machine are similar to the conventional PMV one. Namely, the rotor PM and stator winding magnetic fields in the air-gap are modulated by modulation tooth, and the same order harmonics in the modulated PM and winding magnetic fields are called working harmonics. These working harmonics interact to produce torques. In order to give full play to the magnetic field modulation effects on the improvement of torque, modulation tooth N_f, PM pole-pair P_r and winding pole-pair P_s should satisfy:

$$N_f = P_r + P_s \tag{1}$$

D. Airgap Harmonic Analysis on Torque Performance

Prior to analysis using the flux modulation theory, we made four assumptions:

1) The permeance of steel laminations is unlimited and cannot be saturated.

2) The flux leakage and the effect of finite axial length were disregarded.

3) PMs and air have the same relative permeability.

4) Torque output is approximated as a linear system.

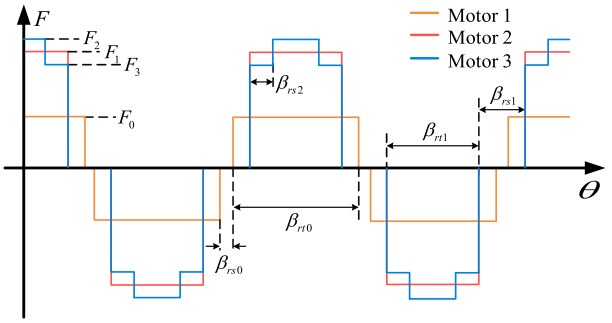

Fig. 6. MMF distribution generated by the PMs.

Fig. 6 illustrates the magnetic motive force (MMF) of the PMs. Their corresponding Fourier series expansion $F(\theta, t)$ can be formulated as:

$$F(\theta,t) = \sum_{i=1,3,5\ldots}^{\infty} F_i \cos iP_r\left(\Omega_r t + \theta\right) \tag{2}$$

where P_r represents PM pole pairs, and Ω_r represents the mechanical rotating velocity. i represents positive odd integer. θ represents airgap circumferential position angle. F_i represents amplitude of the ith-order harmonic in MMF generated by PMs;

$F_{i\text{-Motor 1}}$, $F_{i\text{-Motor 2}}$, and $F_{i\text{-Motor 3}}$ denote the amplitudes of the ith-order harmonic of the three motors.

$$\begin{aligned}
F_{i-\text{Motor1}} &= \frac{4F_0}{i\pi}\sin\left(\frac{i\pi}{2}\right)\cos\left(\frac{\beta_{rs0}iP_r}{2}\right)\\
F_{i-\text{Motor2}} &= \frac{4F_1}{i\pi}\sin\left(\frac{i\pi}{2}\right)\cos\left(\frac{\beta_{rs1}iP_r}{2}\right)\\
F_{i-\text{Motor3}} &= \frac{4F_2}{i\pi}\sin\left(\frac{i\pi}{2}\right)\cos\left[\left(\beta_{rs2}+\frac{\beta_{rs1}}{2}\right)iP_r\right]+\\
&\quad \frac{8F_3}{i\pi}\sin\left(\frac{i\pi}{2}\right)\sin\left[\left(\frac{\beta_{rs1}+\beta_{rs2}}{2}\right)iP_r\right]\sin\left(\frac{\beta_{rs2}iP_r}{2}\right)
\end{aligned} \tag{3}$$

F_0, F_1, F_2, and F_3, respectively, represent MMF step amplitudes. β_{rt1} represents rotor tooth angle. β_{rs1} represents rotor slot angle. β_{rs2} represents ripple reduction region angle. Thus, our proposed methodology can obviously improve the harmonic amplitude of the MMF. In addition, during the calculation, $4\beta_{rs2}=\beta_{rt1}$.

Fourier series expansion of the airgap permeance function in PMV motors were derived using:

$$\Lambda_S(\theta) = \sum_{j=0,\pm1,\pm2\ldots}^{\infty} p_j \cos\left(jN_s\theta\right) \tag{4}$$

where N_s is the number of the stator tooth, j is either zero or a positive integer, and P_j is the amplitude of the jth-order harmonic.

Thus, the airgap flux density of the partitioned design PMV motor can be expressed as,

$$\begin{aligned}B_{\text{Motor3}}(\theta,t) &= F(\theta,t)\Lambda_S(\theta)\\ &= F_{1-\text{Motor3}}P_0\cos\left(P_r\Omega_r t+P_r\theta\right) \quad \rightarrow \textit{Fundamental}\\ &\left.\begin{aligned}&+\frac{1}{2}\sum_{i=1,3,5\ldots}^{\infty}\sum_{j=0,\pm1,\pm2,\ldots}^{\infty}F_{i-\text{Motor3}}P_j\\ &\times\cos\left[iP_r\Omega_r t+\left(jN_s+iP_r\right)\theta\right]\\ &+\frac{1}{2}\sum_{i=1,3,5\ldots}^{\infty}\sum_{j=0,\pm1,\pm2,\ldots}^{\infty}F_{i-\text{Motor3}}P_j\\ &\times\cos\left[iP_r\Omega_r t+\left(jN_s-iP_r\right)\theta\right]\end{aligned}\right\} \textit{Rich harmonics}\end{aligned} \tag{5}$$

Based on the Fourier series, the airgap magnetic flux density radial component B_r and tangential component B_t can be expanded

$$\begin{aligned}B_r(\theta,t) &= \sum_q B_{rq}\cos\left[q\theta-\theta_{rq}(t)\right]\\ B_t(\theta,t) &= \sum_q B_{tq}\cos\left[q\theta-\theta_{tq}(t)\right]\end{aligned} \tag{6}$$

where B_{rq} and B_{tq} are the qth Fourier coefficients of radial component B_r and tangential component B_t expanded by Fourier series, $\theta_{rq,}$ and θ_{tq} are the phase of qth airgap harmonic.

Using the classical motor theory, the electromagnetic torque generated by qth-order harmonic were estimated on the basis of [14]-[15]

$$T_{outq}(t)=\frac{\pi R^2 l_{ef}}{\mu_0}B_{rq}B_{tq}\cos\left(\theta_{rq}(t)-\theta_{tq}(t)\right) \tag{7}$$

where R is the radius of the air gap, l_{ef} is the motor shaft length, and μ_0 is the vacuum permeability.

Meanwhile, the ripple of the torque generated by the qth-order harmonic can be expressed as

$$T_{rq}(t)=\frac{\text{Max}\left(T_{\text{out}q}(t)\right)-\text{Min}\left(T_{\text{out}q}(t)\right)}{\text{Avg}\left(T_{\text{out}q}(t)\right)} \tag{8}$$

where Max($T_{\text{out}q}$ (t)), Min($T_{\text{out}q}$ (t), and Avg($T_{\text{out}q}$ (t)) are the maximum value, minimum value, and average value of output torque generated by the qth-order harmonic, respectively.

Based on (7) and (8), the output torque amplitude of the PMV motors was estimated using the following:

$$T_{\text{out}}(t)=\sum_q T_{\text{out}q}(t)=\frac{\pi R^2 l_{ef}}{\mu_0}\sum_q B_{rq}B_{tq}\cos\left(\theta_{rq}(t)-\theta_{tq}(t)\right) \tag{9}$$

Similarly, torque ripples were assessed using

$$T_r(t)=\sum_q T_{rq}(t)=\frac{1}{\sum_q B_{rq}B_{Tq}\cos\left[\theta_{rq}(t)-\theta_{tq}(t)\right]}\times\left\{\text{Max}\left(\sum_q B_{rq}B_{Tq}\cos\left[\theta_{rq}(t)-\theta_{tq}(t)\right]\right)-\text{Min}\left(\sum_q B_{rq}B_{Tq}\cos\left[\theta_{rq}(t)-\theta_{tq}(t)\right]\right)\right\} \tag{10}$$

as its optimizing strategies implemented, based on which we determined the objectives, design variables, and optimization. Then, we assessed the motor's leading airgap flux harmonics. We chose an airgap harmonic possessing a significant contribution to the output torque and optimizing parameters of the torque enhancement region. Finally, simulations were conducted to validate the obtained optimization-related results.

III. Torque Performance Optimization Considering Partitioned Design

Section II suggests that the torque design region of the airgap flux harmonics significantly influenced torque output and corresponding ripples. Fig. 7 illustrates our proposed airgap-harmonic-oriented partitioned design method, as well

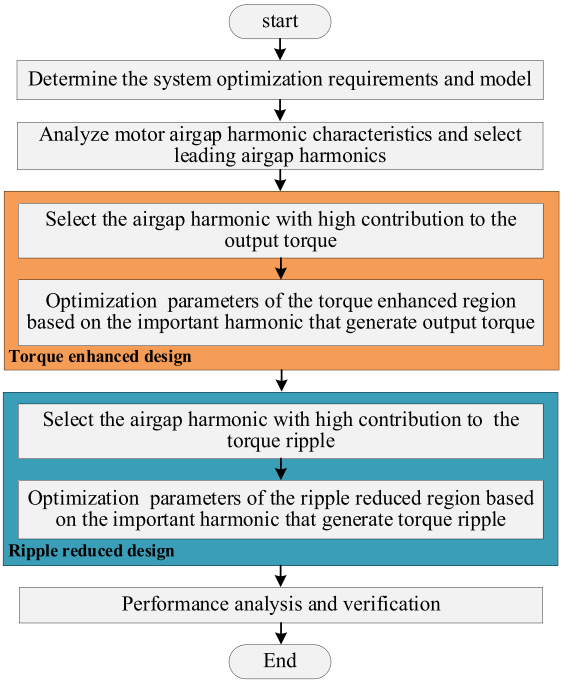

Fig. 7. Flowchart of the airgap-harmonic-oriented partitioned design method.

A. Output Torque Enhancement

For the initial motor, the main airgap flux harmonics of the no-load flux density are selected (Fig. 8). It is noted that on the principle of flux-modulation, the fundamental of the initial motor is 19th.

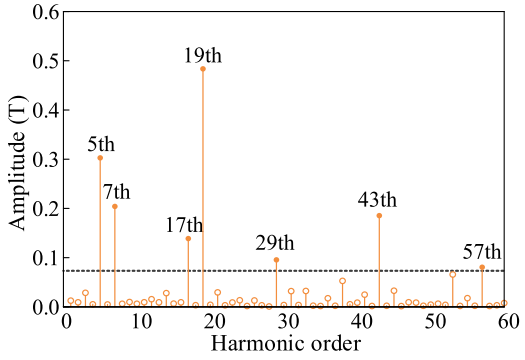

Fig. 8. The main airgap density harmonics of motor 1.

On the basis of maxwell stress tensor method (MSTM), Motor 1 main torque output is generated by the 19th harmonic, while other harmonics did not have significant effects (Fig. 9(a)). Therefore, the 19th harmonic is selected as the

optimization target of the torque enhancement region. Fig. 9(b) shows that the output torque generated by the 19th harmonic increases with increasing h_t, but then decreased when α_t increases. According to the variation trend, h_t and α_t can be 9.4mm and 3deg to yield larger output torque, respectively.

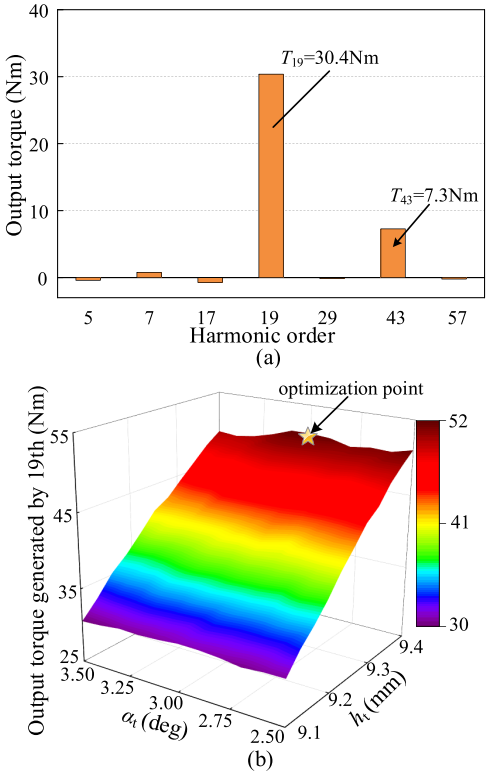

Fig. 9. (a) Contribution of airgap flux harmonics to the output torque of Motor 1. (b) Variation relationships of α_t, h_t and output torque generated by 19th harmonic.

B. Torque Ripple Suppression

Through the design of the torque enhancement region, the output torque is greatly improved, but it also increases torque ripple. We assessed the effects of the airgap flux harmonics on torque ripple (Fig. 10(a)) and found that the 29th harmonic primarily influenced the torque ripple of Motor 2. On this basis, the ripple reduction region is optimized in Fig. 10(b). To determine low torque ripple while retaining the value of output torque, h_r and α_r are chosen to be 1.2mm and 0.75deg, respectively.

In addition, the performance comparison among these motors is shown in Table II. In the meantime, we compared various harmonics' output torque and torque ripple to confirm

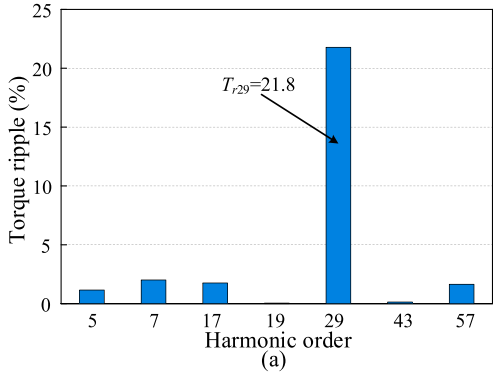

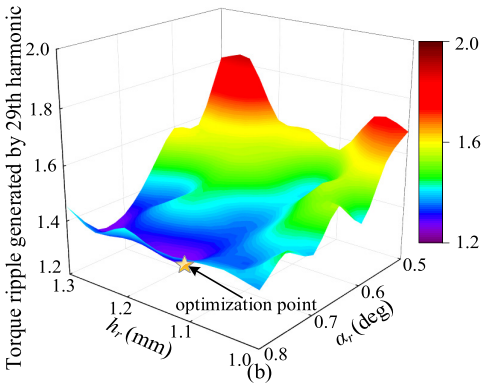

Fig. 10. (a) Contribution of airgap flux harmonics to torque ripple of Motor 2. (b) Variation relationships of α_r, h_r and torque ripple generated by 29th harmonic.

TABLE II
PERFORMANCE COMPARISONS

Performance	Motor 1	Motor 2	Motor 3
Output torque (Nm)	38.5	70.3	70.8
Torque ripple (%)	3.6	5.4	2.1
Torque generated by 19th harmonic (Nm)	30.4	51.1	51.1
Ripple generated by 29th harmonic (%)	0.6	21.8	1.4

the optimization. Fig. 11(a)-(b) shows that the 19th airgap harmonic in Motor 2 increased output torque by 68.1% comp ared to Motor 1, while other harmonics had little effects on torque output. Additionally, torque ripple was decreased from 5.4% to 2.1% because of the considerably reduced torque ripple of the 29th harmonic. Altogether, these validate the promising ability of our proposed airgap harmonic-oriented partitioned design method.

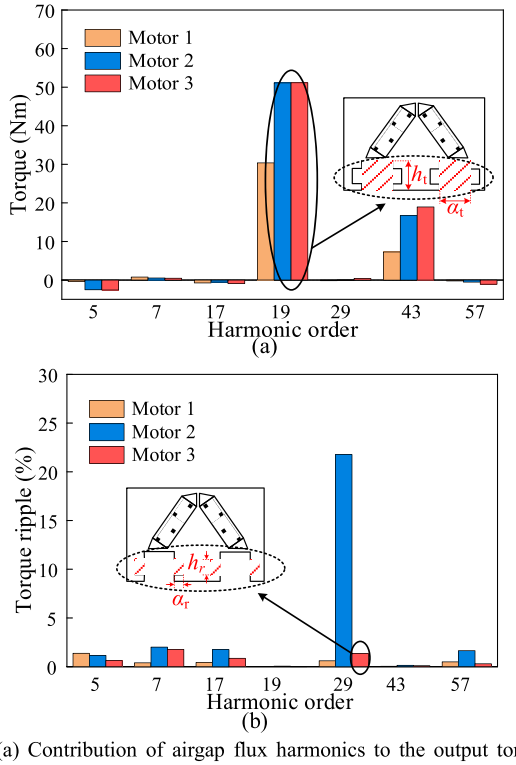

Fig. 11. (a) Contribution of airgap flux harmonics to the output torque. (b) Contribution of airgap flux harmonics to the torque ripple.

IV. Performance Analysis And Comparison

Here, we assessed the electromagnetic performances of three FEM-based models of Motor 1, Motor 2, and Motor 3 on the basis of their average output torque, torque ripple, no-load flux distribution, and back-EMF.

Firstly, the no-load magnetic field and flux distributions of the three motors are described in Fig. 12(a)-(c). It is observed that there exists no magnetic saturation phenomenon in most areas of Motor 1 and Motor 2, which means the better operation of the two motors.

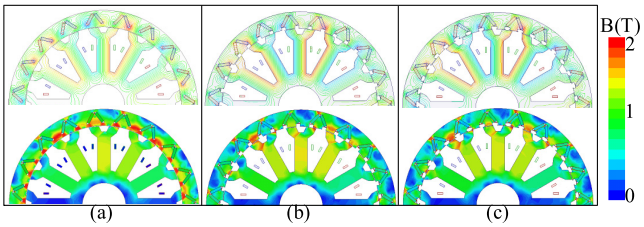

Fig. 12. Magnetic field and flux distribution of motors. (a) Motor 1. (b) Motor 2. (c) Motor 3.

Fig. 12 shows the no-load airgap flux density waveforms of the three motors. It should be noted that, due to a large number of pole pairs of the PM rotor, Fig. 13(a) shows the waveforms of the half period. It can be seen that the airgap flux density waveform marked with a rectangle is significantly enhanced after the torque enhancement region design. The torque enhancement region design can effectively increase the maximum value of the flux density and thus is expected to increase the output torque. Similarly, the local peak value of motor 3, marked by an ellipse in Fig. 13(a), is lower than the other two motors, implying that the ripple reduction region design indeed enhanced the airgap's stored magnetic field energy to reduce torque ripple. Fig. 13(b) shows the comparisons of the main harmonic spectrum between motor 1, motor 2, and motor 3, showing that our proposed partitioned designs remarkably increased the amplitude of the main harmonics.

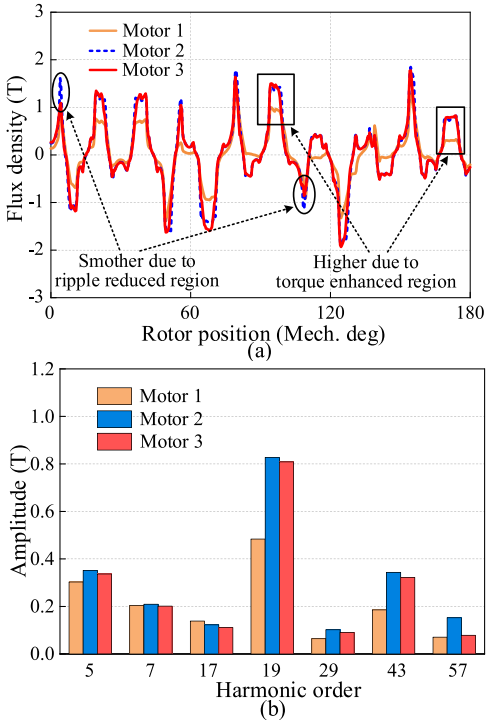

Fig. 13. Comparison of air-gap flux density. (a) Airgap flux density distributions. (b) Airgap flux density amplitudes.

Then, Fig. 14(a) illustrates their no-load back-EMF waveforms and indicates that those with torque enhancement region had higher back-EMF amplitude compared to the initial motor (99.1% versus 82.3%, respectively), indicating the generation of greater torque. However, spectrum analysis shows that partitioned designed motor had a higher total harmonic distortion (THD), which deserves follow-up studies.

Fig. 14(b) shows that the proposed airgap-harmonic-orientated partitioned design method led to a significant improvement in torque performance. The torque enhancement region design led to an average torque output of 70.8Nm, which is increased by 80% primarily because of the optimal design of harmonic19th. Although this also leads to an increase in torque ripple, primarily influenced by the 29th harmonic. Through designing the ripple reduction region, the torque ripple is decreased by 61.1% to 2.1%.

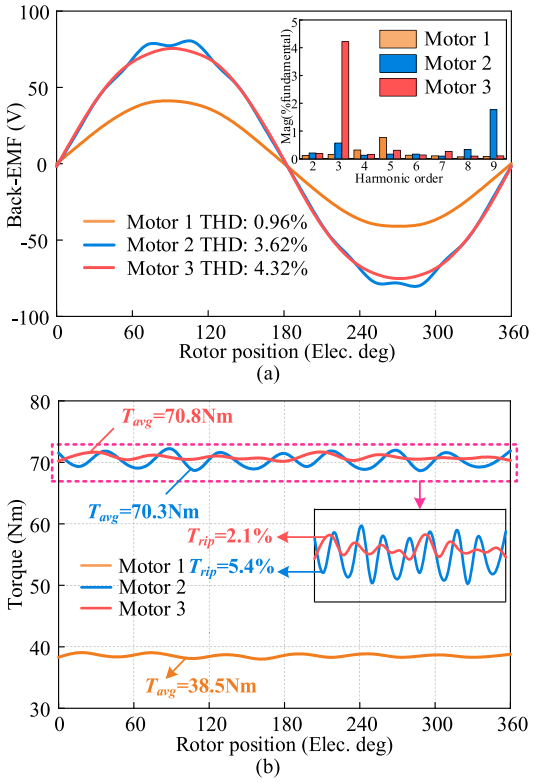

Fig. 14. (a) No-load back EMF waveforms. (b) Torque performances.

V. Conclusion

This research study proposes an airgap-harmonic-orientated partitioned design method for PMV motors. For better presentation, the conclusions are summarized as follows.

1) By theoretical analysis and calculation, it is found that 19 harmonics affected output torque, and 29 harmonics affected torque ripple in the partitioned PMV motor, thereby yielding enhanced torque output and ripples in the motor and laying a foundation for the realization of synchronous improvement of torque performances in this paper.

2) By finding the regions which significantly influence the

main harmonics of torque output and ripples, respectively, used for the design regions of their respective targets. By the analysis of the optimization results, the proposed partitioned design can effectively realize the synchronous improvement of torque and pulsation, which provides novel insights for efficiently designing an improved PMV motor.

3) Finally, results based on the finite element method showed that our proposed partitioned design motor led to improved output torque by nearly 80% compared to the initial motor. In comparison, torque ripple is reduced to 2.1%. Thus, our proposed airgap-harmonic-oriented partitioned design could be considered for high-torque performance PMV motors.

REFERENCES

[1] K. Xie, D. Li, and R. Qu *et al*, "A new perspective on the PMV machine mechanism," *IEEE Trans. Ind. Appl.*, vol. 55, no. 2, pp. 1420-1429, March/April 2019.

[2] C. Gan, N. Jin, and Q. Sun *et al*, "Multiport bidirectional SRM drives for solar-assisted hybrid electric bus powertrain with flexible driving and self-charging functions," *IEEE Trans. Power Electron.*, vol. 33, no. 10, pp. 8231–8245, Oct. 2018.

[3] W. Ding, S. Yang, and Y. Hu *et al*, "Design consideration and evaluation of a 12/8 high-torque modular-stator hybrid excitation switched reluctance machine for EV applications," *IEEE Trans. Ind. Electron.*, vol. 64, no. 12, pp. 9221–9232, Dec. 2017.

[4] D. Fan, L. Quan, and X. Zhu *et al*, "Airgap-Harmonic-Based multilevel design and optimization of a Double-Stator flux modulated permanent magnet motor," *IEEE Trans. Ind. Electron.*, vol. 68, no. 11, pp. 10534-10545, Nov. 2021.

[5] L. Cao, K. T. Chau, and C. H. T. Lee *et al*, "Design and analysis of a new Parallel-Hybrid-Excited machine with Harmonic-Shift Structure," *IEEE Trans. Ind. Electron*., vol. 67, no. 3, pp. 1759-1770, March 2020.

[6] B. Lee, Z. Q. Zhu, and L. Huang, "Investigation of torque production and torque ripple reduction for Six-Stator/Seven-Rotor-Pole variable flux reluctance machines," *IEEE Trans. Ind. Appl.*, vol. 55, no. 3, pp. 2510-2518, May/June 2019.

[7] Z. Xiang, X. Zhu, and L. Quan *et al*, "Multilevel design optimization and operation of a brushless double mechanical port Flux-Switching Permanent-Magnet motor," *IEEE Trans. Ind. Electron.*, vol. 63, no. 10, pp. 6042-6054, Oct. 2016.

[8] W. H. Tai, M. C. Tsai, and Z. L. Gaing *et al*, "Novel stator design of double salient permanent magnet motor," *IEEE Trans. Magn*., vol. 50, no. 4, pp. 1-4, April 2014.

[9] L. Fang, D. Li, and X. Ren *et al*, "A novel permanent magnet vernier machine with coding-shaped tooth," *IEEE Trans. Ind. Electron.*, vol. 69, no. 6, pp. 6058-6068, June 2022.

[10] L. Jia, M. Lin, and W. Le *et al*, "Dual-Skew magnet for cogging torque minimization of axial flux PMSM with segmented stator," *IEEE Trans. Magn*., vol. 56, no. 2, pp. 1-6, Feb. 2020.

[11] M. Zhou, X. Zhang, and W. Zhao *et al*, "Influence of magnet shape on the cogging torque of a surface-mounted permanent magnet motor," *Chin. J. Electr. Eng*., vol. 5, no. 4, pp. 40-50, Dec. 2019.

[12] C. Gan, J. Wu, and M. Shen *et al*, "Investigation of short permanent magnet and stator flux bridge effects on cogging torque mitigation in FSPM machines," *IEEE Trans. Energy Convers.*, vol. 33, no. 2, pp. 845-855, June 2018.

[13] Y. Zeng, M. Cheng, and G. Liu *et al*, "Effects of magnet shape on torque capability of Surface-Mounted permanent magnet machine for servo applications," *IEEE Trans. Ind. Electron*., vol. 67, no. 4, pp. 2977-2990, April 2020.

[14] Z. Z. Wu and Z. Q. Zhu, "Analysis of Air-Gap field modulation and magnetic gearing effects in switched flux permanent magnet machines," *IEEE Trans. Magn.*, vol. 51, no. 5, pp. 1-12, May 2015.

[15] A. Fatemi, N. Demerdash, and T. W. Nehl *et al*, "Large-scale design optimization of PM machines over a target operating cycle," *IEEE Trans. Ind. Appl.*, vol. 52, no. 5, pp. 3772–3782, Sep./Oct. 2016.

Zhaopeng Wu received the B.Sc Nanjing University of Information Science & Technology Binjiang College, Nanjing, China, in 2020, where he is currently working toward the master's degree in electrical engineering.

His current research interests include design and analysis of flux-modulated permanent magnet machines for electric vehicles (EVs).

Li Quan received the B.Sc. Degree in electrical engineering from Hefei University of Technology, Hefei, China, in 1985, the M.Sc. Degree in motors and electrical specialty from Southeast University, Nanjing, China, in 1991, and the Ph.D. degree in power electronics and power transmission from Nanjing University of aeronautics and astronautics in 2007.

Since 1998, he has been with Jiangsu University, where he is currently a professor in the School of Electrical and Information Engineering. He has authored or coauthored more than 100 technical papers, one textbook, and holds three patents in these areas. His teaching and research interests include high performance permanent magnet motor for electric vehicles (EVs), double rotor permanent magnet motor for hybrid electric vehicles (HEVs) and motor drives control.

Zixuan Xiang received the B.Sc. degree from Hubei Polytechnic University, Huangshi, China, in 2010， the M.Sc. and the Ph.D. degrees in power electronics and power transmission from the School of Electrical and Information Engineering, Jiangsu University, Zhenjiang, China, in 2017.

He is currently an associate professor with the School of Electrical and Information Engineering, Jiangsu University. His main research interests include design, optimization, and drive control of high-performance permanent magnet motor and novel double mechanical port permanent magnet motor for application in modern electric vehicles (EVs) and hybrid electric vehicles (HEVs).

Deyang Fan received the B.Sc. degree in electrical engineering from North China Electric Power University, Baoding, China, in 2014, and the Ph.D. degree in electrical engineering from Jiangsu University, Zhenjiang, China in 2021. From 2019 to 2020, he was with the Department of Electrical and Computer Engineering, University of Kentucky, Lexington, KY, USA, as a Joint Ph.D. Student.

He is currently a lecturer in School of Electrical and Information Engineering, Jiangsu University. His current research interests include modeling, design, optimization, and control of high-performance permanent magnet motors for electric vehicles.

Tengguang Wang received the B. Sc. degree in electrical engineering from Jiangsu University, Zhenjiang, China, in 2017, where he is currently working towards the Ph. D. degree in electrical engineering.

His current research interests include design and analysis of flux-modulated permanent magnet machines for electric vehicles.

Xiaoyong Zhu (M'09) received the B.Sc. and M.Sc. degrees in electrical engineering from Jiangsu University, Zhenjiang, China, in 1997 and 2002, respectively, and the Ph. D degree from the School of Electrical Engineering, Southeast University, Nanjing, China, in 2008. During the period of doctoral study, his subject is electrical engineering, which mainly focuses on the design, analysis and control of the type of hybrid-excited permanent magnet machine.

He has been with Jiangsu University since 1999, where he is currently a Professor with the School of Electrical Information Engineering. In 2007 to 2008, he was a Research Assistant with the Department of Electrical and Electronic Engineering, University of Hong Kong. From 2012 to 2013, he was a Visiting Professor with the Department of Energy-Funded Graduate Automotive Technology Education Center for Electric Drive Transportation, University of Michigan, Dearborn, Michigan, USA. His current research interests include design and drive control of electric machines with wide-speed range, less rare-earth permanent magnet motor, and multi-port permanent magnet motor. In these areas, he has authored and co-authored more than 70 referred technical papers, and holds 12 patents.